Supplementary Materials:

S1. Below, a concise explanation of the experimental data utilized for validating the model is presented:

-Batool (2015) tested cement-based foams by considering three levels of densities range: 400, 600 and 800 kg/m3. The work provided thermal conductivities in low, middle, and high-porosities foams. The effect of replacing fly-ash, silica fume, and metakaolin, up to 20% by weight was also investigated to examine their influences on the thermal conductivity. In the study, the prominent pore size for the three densities, 800, 600 and 400, was shown to be 0.03 to 0.07 mm.

-Awang et al. (2012) investigated the effects of different percentages of fly ash, lime and hydrophobic polypropylene fibres on the microstructure formation and thermal properties of lightweight foamed concrete. Three different densities of 600, 1000 and 1400 kg/m3 were considered.

-Wei et al. (2013) provided a comprehensive experimental and numerical analysis of foamed concretes with a large range of densities (300-1700 kg/m3). A microstructure-based numerical model was proposed to predict the effective thermal conductivity of the foams with different porosities. The effect of convection and radiation on heat transfer for high and low porosity foamed concretes were also evaluated. The author unveiled that heat transfer due to convection can be neglected, because of the presence of predominantly closed-cell pores (smaller than 4 mm), while the radiation heat transfer was found to be a non-negligible factor for porosities higher than 85%. Under standard air pressure conditions and at 293 K, radiation contributed to approximately 6% of the overall heat transfer in these high porosity concretes.

-Mydin (2011) conducted an experimental study on the effect of porosity and pore size on the thermal conductivity of foam concretes with seven variable densities (650, 700, 800, 900, 1000, 1100 and 1200 kg/m3). The dominant pore size for densities between 650 and 1200 kg/m3 was reported to be between 0.72 and 0.48 mm respectively. It was also shown that a reduction in foam density by 100 kg/m3 leads to a decrease of the thermal conductivity by 0.04 W/mK.

-Davraz et al (2016) presented a study on the correlation between dry densities, running from 350 to 1500 kg/m3, and thermal conductivity of foam concretes with fine limestone and polypropylene fibers.

-Oren et al. (2020) evaluated the thermo-physical properties of nine different foam concretes containing different volumetric amount of fly ash (FA) as binder, and granulated blast furnace slag (GBS) as fine aggregate by increasing the w/b ratio from 0.55 to 0.91. The study provides an in-depth analysis of the foam microstructure to explain the obtained experimental results.

-Jiang et al. (2017) & (2016) studied the effects of waterborne epoxy resin, silica fume and metakaolin on air-void structure and thermal conductivity in high porosity (> 90%) foams. The results indicated the presence of pore diameters less than 2.5 mm in all tested samples. When fine particles of SF (≤1 μm) and MK (1.0-9.5 μm) were added to the high porosity foams, the interparticle spacing would be reduced. The latter increased the real viscosity of the cement paste, depressed the bleeding, and accelerated the overlapping of particles These effects play a crucial role in stabilizing foams for producing highly porous cementitious systems with smaller bubbles, and ultimately leading to a decrease in thermal conductivity.

	Ultra-light	Low-density	Moderate strength	Structural
Compressive strength (MPa)	< 1	1-12	2-27	4-60
Elastic modulus (GPa)	< 1	1-4	2-6	4-18
Shrinkage (%)	> 0.3	0.2-0.3	1.1-0.2	< 0.1

Figure S1. foam type vs. properties classification according to.

S2. Air-void shape/packing is determined based on the pore shape structure of cementitious foam, as shown in Figure 3. The packing is chosen according to the corresponding shape from the table below.

Table S1. Maximum packing fractions Φ_m for disperse phase with different shape and type of packing .

Shape of dispersed phase	Type of packing	Maximum Packing fraction Φ_m
Spheres	Hexagonal close	0.7405
Spheres	Face centered cubic	0.7405
Spheres	Body centered cubic	0.60
Spheres	Simple cubic	0.524
Spheres	Random close	0.637
Spheres	Random loose	0.601
Rods or fibers	Uniaxial hexagonal close	0.907
Rods or fibers	Uniaxial simple cubic	0.785
Rods or fibers	Uniaxial random	0.82
Rods or fibers	Three dimensional random	0.52

Table S2. Value of A for Various Two-Phase Systems according to .

Shape/Type of dispersed phase	Direction of heat flow	A
Spheres	Any	1.5
Aggregates of spheres	Any	2.5/ Φ_m -1
Randomly oriented rods, Aspect ratio = 2	Any	1.58
Randomly oriented rods, Aspect ratio = 4	Any	2.08
Randomly oriented rods, Aspect ratio = 6	Any	2.8
Randomly oriented rods, Aspect ratio = 10	Any	4.93
Randomly oriented rods, Aspect ratio = 15	Any	8.38
Uniaxially oriented fibers	Parallel to fibers	2L/D
Uniaxially oriented fibers	Perpendicular to fibers	0.5

S3. Figures S2–S8 show the homogenized predicted conductivity values plotted against the employed data, analyzed author by author. The figures display both the linear regression lines and the square root errors. The prediction results show promising outcomes, with high R^2 values: e.g., 0.9756 for the Batool dataset , 0.9937 for Awang et al. , 0.9994 for Wei et al. , 0.9673 for Mydin , 0.9787 for Davraz et al. , 0.9793 for Oren et al. and 0.8957 for Jiang et al. .

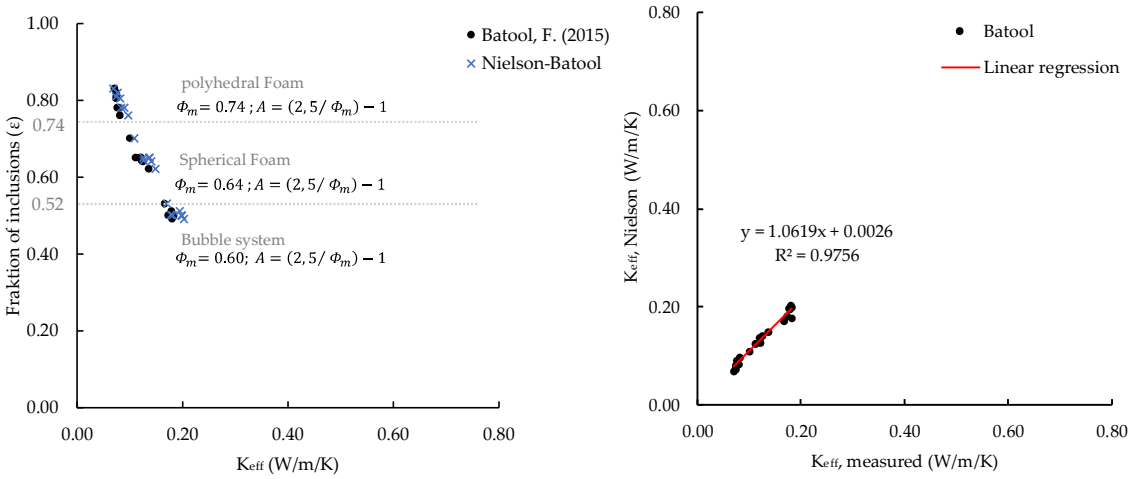

Figure S2. Lewis–Nielsen predictions vs. Batool data: comparison and linear regression + R2.

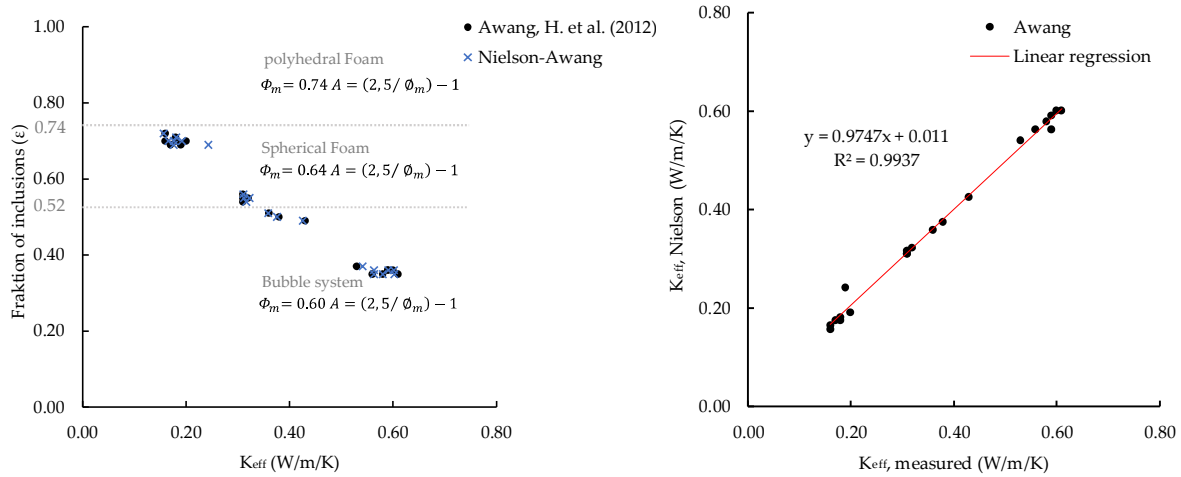

Figure S3. Lewis–Nielsen predictions vs. Awang data: comparison and linear regression + R2.

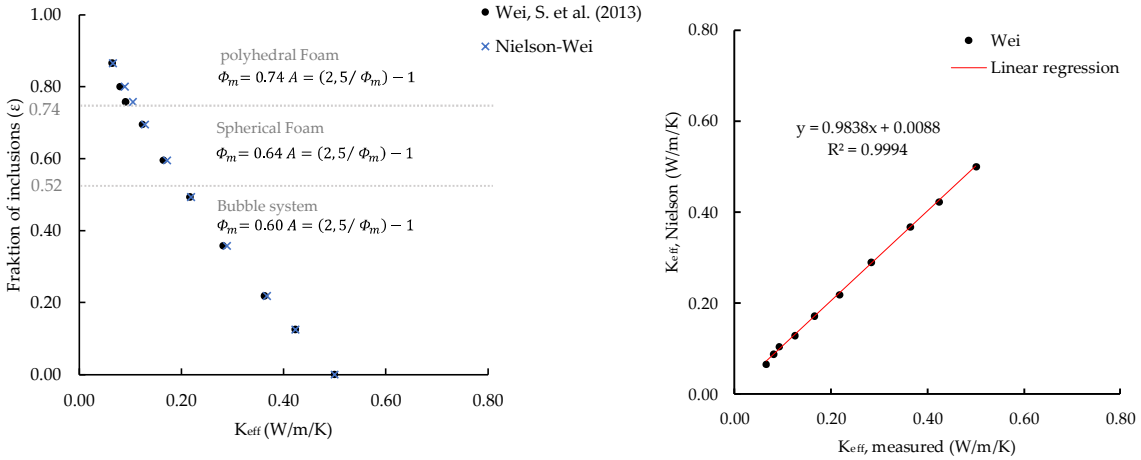

Figure S4. Lewis–Nielsen predictions vs. Wei data: comparison and linear regression + R2.

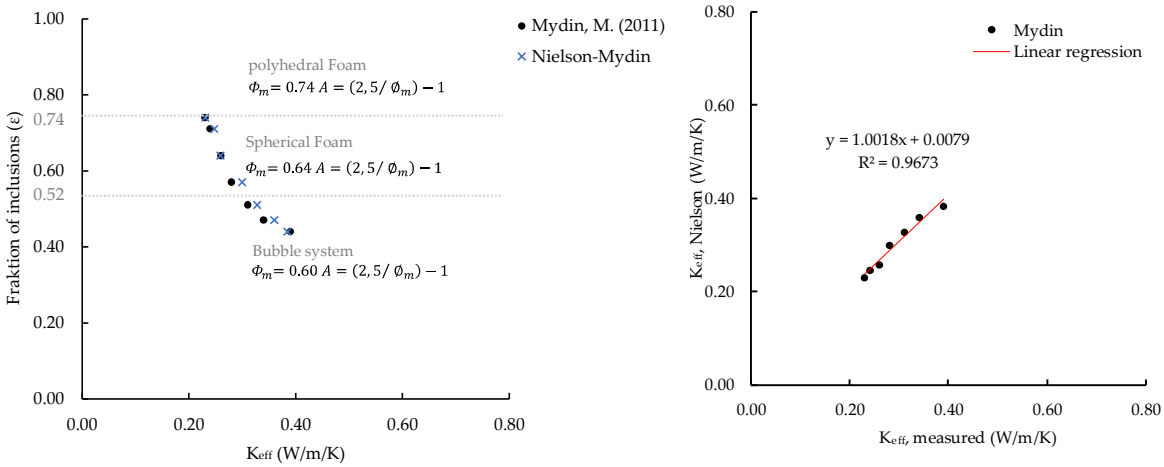

Figure S5. Lewis–Nielsen predictions vs. Mydin data: comparison and linear regression + R2.

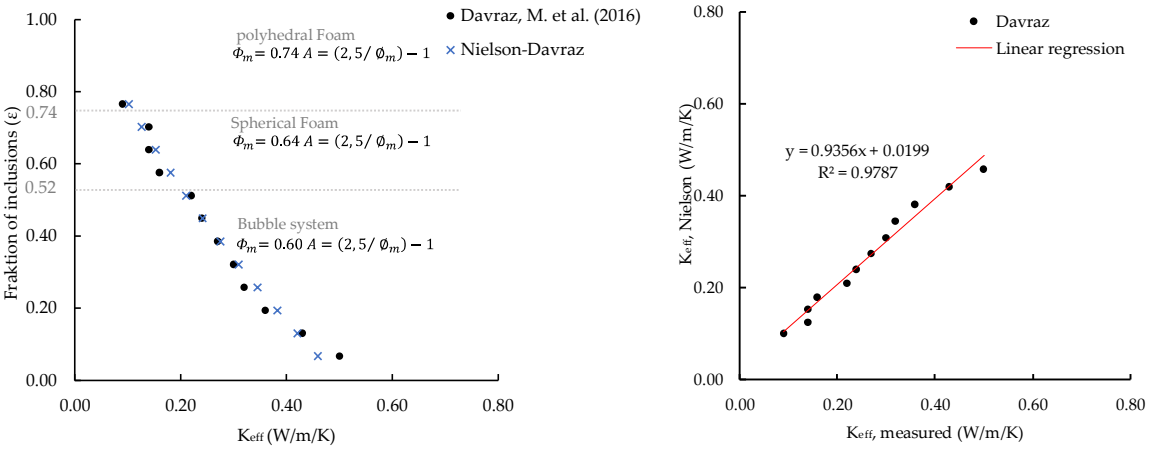

Figure S6. Lewis–Nielsen predictions vs. Davraz data: comparison and linear regression + R2.

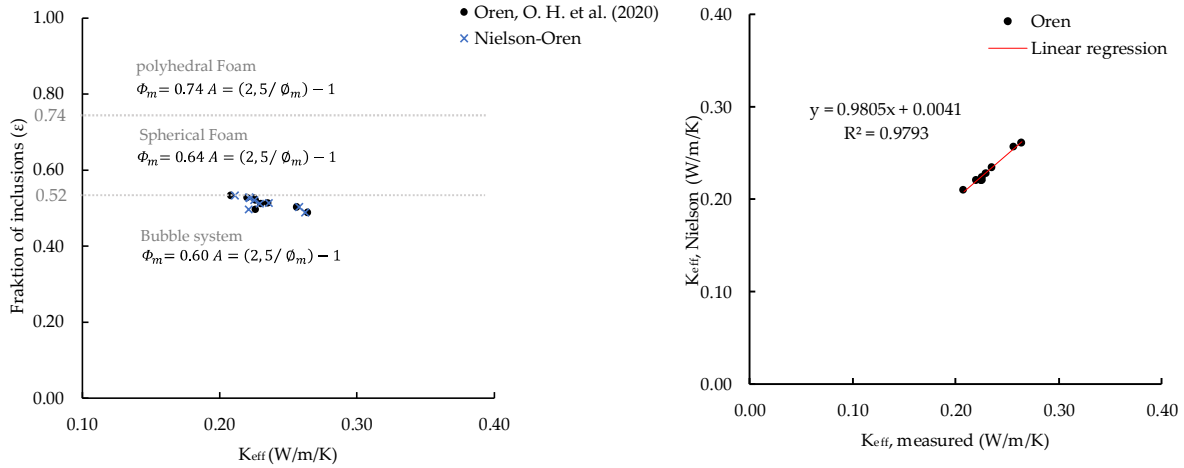

Figure S7. Lewis–Nielsen predictions vs. Oren data: comparison and linear regression + R2.

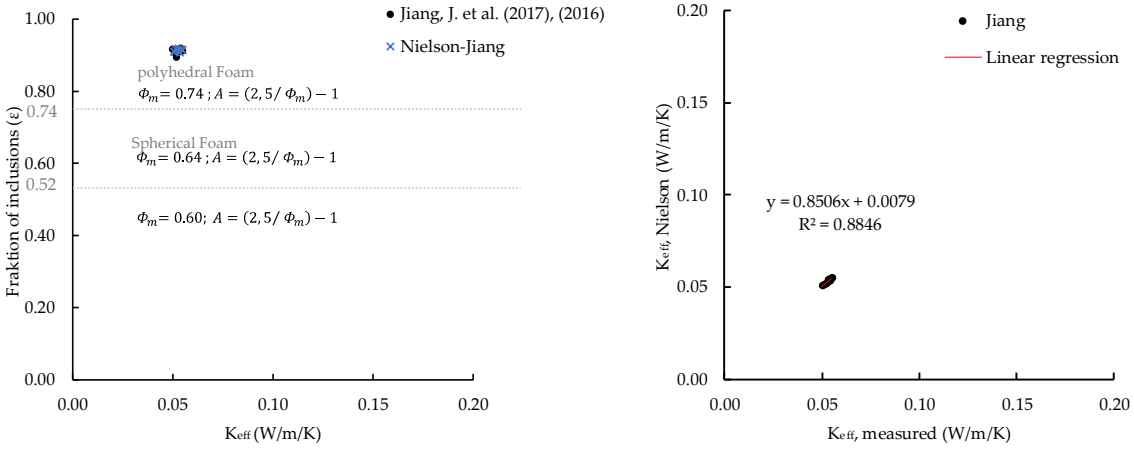

Figure S8. Lewis–Nielsen predictions vs. Jiang et al. (2017) & (2016): comparison and linear regression + R2.

S4. The overall heat transfer in foamed concretes, like in any porous media, is the result of three different mechanisms: conduction, convection, and radiation. The latter include both the heat conduction in cementitious matrix/skeleton together with the heat conduction, convection, and radiation within the air-fraction. In porous cementitious foam systems, heat transfer due to convection in air-voids can be neglected. Also, the effect of air radiation at low porosity is not relevant. The radiation contribution could only be an issue when the air volume fraction is over 85%.

Thermodynamics principles

The equation describing a heat transfer (conduction-only) problem can be written as:

$$\frac{\partial Q}{\partial t} = \nabla.(k\nabla T) + \dot{q}_v \forall \mathbf{x} \in \Omega \quad (1)$$

being Q the heat of the system (time dependent, t), k is the thermal conductivity (which depends on temperature T and position $\mathbf{x}$ of the considered body Ω), $\dot{q}_v$ represents the possible source term, finally $\nabla.$ and ∇ are the divergence and gradient operators, respectively, of the Fourier's law of heat in Eq. (1).

To solve thermal problems involving phase changes, applicable for cementitious composites in building physics problems, the above equation of heat conduction can be written as follows:

$$\frac{\partial H}{\partial t} = \nabla.(k\nabla T) + \dot{q}_v \quad \forall \boldsymbol{x} \in \Omega \quad (2)$$

describing the heat conduction through a wall.

Eq. (1) can be simplified and re-written in one dimensional format as:

$$q_x = -k\, A \frac{dT}{dx} \quad (3)$$

being q_x the one dimensional heat flux (time dependent as well, t), A is the face area and dT/dx is the temperature gradient and measures how temperature changes with position x.

Enthalpy-based and Apparent Calorific Capacity Method

For simulating thermal storage phenomena in porous cementitious foam composites, the Apparent Calorific Capacity (ACCM) is a simple method, based on the assumption that the schematized material acts as a homogenous medium and can be applied to simulate phase change processes. The latter provides a description of the enthalpy evolution of a system in terms of an apparent heat capacity (including the latent heat in the specific heat) during thermal phase changes. Thus, starting from Eq. (2), commonly known as the enthalpy-based method, and adopting the following chain rule:

$$\frac{\partial H}{\partial t} = \frac{\partial H}{\partial T}\frac{\partial T}{\partial t} \quad (4)$$

and by introducing the so-called temperature-dependent apparent heat capacity, defined as:

$$\frac{\partial H}{\partial T} = \rho C_{p,eff}(T) \quad (5)$$

hence, Eq. (2) modifies into the following non-linear ACCM transient heat equation:

$$\rho C_{p,eff}(T)\frac{dT}{dt} = \nabla.(k\nabla T) \quad (6)$$

To complete the above problem statement of the ACCM approach, Initial (ICs) and Boundary Conditions (BCs) need to be employed, as defined here below:

$$T(x,t) = T_0 \quad \text{when t=0}$$
$$T(x,t) = T_{left} \quad \text{at } x = L$$
$$T(x,t) = T_{right} \quad \text{at } x = 0$$